pubs.acs.org/acschemicalbiology

Articles

Real-Time Cellular Thermal Shift Assay to Monitor Target Engagement

Tino W. Sanchez,[†] Michael H. Ronzetti,[†] Ashley E. Owens, Maria Antony, Ty Voss, Eric Wallgren, Daniel Talley, Krishna Balakrishnan, Sebastian E. Leyes Porello, Ganesha Rai, Juan J. Marugan, Samuel G. Michael, Bolormaa Baljinnyam, Noel Southall, Anton Simeonov, and Mark J. Henderson*

Cite This: *ACS Chem. Biol.* 2022, 17, 2471−2482

Read Online

ACCESS | Metrics & More | Article Recommendations | Supporting Information

ABSTRACT: Determining a molecule's mechanism of action is paramount during chemical probe development and drug discovery. The cellular thermal shift assay (CETSA) is a valuable tool to confirm target engagement in cells for a small molecule that demonstrates a pharmacological effect. CETSA directly detects biophysical interactions between ligands and protein targets, which can alter a protein's unfolding and aggregation properties in response to thermal challenge. In traditional CETSA experiments, each temperature requires an individual sample, which restricts throughput and requires substantial optimization. To capture the full aggregation profile of a protein from a single sample, we developed a prototype real-time CETSA (RT-CETSA) platform by coupling a real-time PCR instrument with a CCD camera to detect luminescence. A thermally stable Nanoluciferase variant (ThermLuc) was bioengineered to withstand unfolding at temperatures greater than 90 °C and was compatible with monitoring target engagement events when fused to diverse targets. Utilizing well-characterized inhibitors of lactate dehydrogenase alpha, RT-CETSA showed significant correlation with enzymatic, biophysical, and other cell-based assays. A data analysis pipeline was developed to enhance the sensitivity of RT-CETSA to detect on-target binding. RT-CETSA technology advances capabilities of the CETSA method and facilitates the identification of ligand-target engagement in cells, a critical step in assessing the mechanism of action of a small molecule.

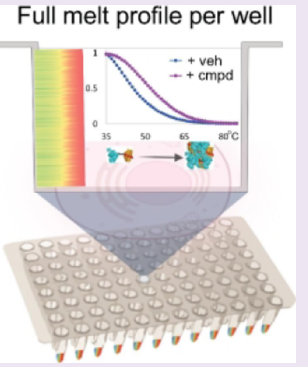

INTRODUCTION

The cell is a complex environment with numerous, tightly controlled biochemical reactions and interactions between cellular components.[1] Proteins are central to many cellular processes, and there is indispensable value in identifying small molecules that target the proteome with high specificity and affinity. Confirming the engagement between a protein target and small molecule under physiologically relevant conditions poses a substantial challenge in early-stage drug discovery and probe development. Most strategies to study target engagement are labor-intensive, low-throughput, or do not provide evidence of ligand-target binding in a physiological, cellular environment.[2] The gold standard for target engagement remains co-crystallization of target and ligand using X-ray crystallography, but this methodology remains highly complex, is not amenable to all target classes, and is not suitable for testing large numbers of compounds. Sensor-based biophysical methods like isothermal calorimetry and surface plasmon resonance (SPR) detect direct target binding but implement simplified acellular conditions and require significant amounts of purified protein and assay optimization.[3,4] Thermal shift-based biochemical methods, such as differential scanning fluorimetry (DSF), also use recombinant protein to detect ligand-induced thermal shifts by measuring changes in hydrophobic dyes or intrinsic protein fluorescence (nanoDSF).[5−7] None of these approaches account for complexities found in cells, including membrane barriers and the potential for off-target binding.

The cellular thermal shift assay (CETSA) allows for the study of target engagement with a small molecule or biomolecule in intact cellular environments, linking observed phenotypic responses with a compound's molecular target.[8,9] CETSA can support direct target engagement by detecting a thermodynamic (de)stabilization of a protein resulting from ligand binding that alters discrete bond energy and shifts the Gibbs free energy of the system. This shift in system energy can be detected by measuring the aggregation properties of the target protein when a thermal challenge is applied.[10] Traditionally, the CETSA method is performed as a label-free lytic end-point assay, requiring individual samples to be prepared for each temperature or compound concentration. After incubating cells with a compound of interest, samples are heated to discrete temperatures and the unfolded aggregated

Received: April 16, 2022
Accepted: August 19, 2022
Published: September 1, 2022

https://doi.org/10.1021/acschembio.2c00334
ACS Chem. Biol. 2022, 17, 2471−2482

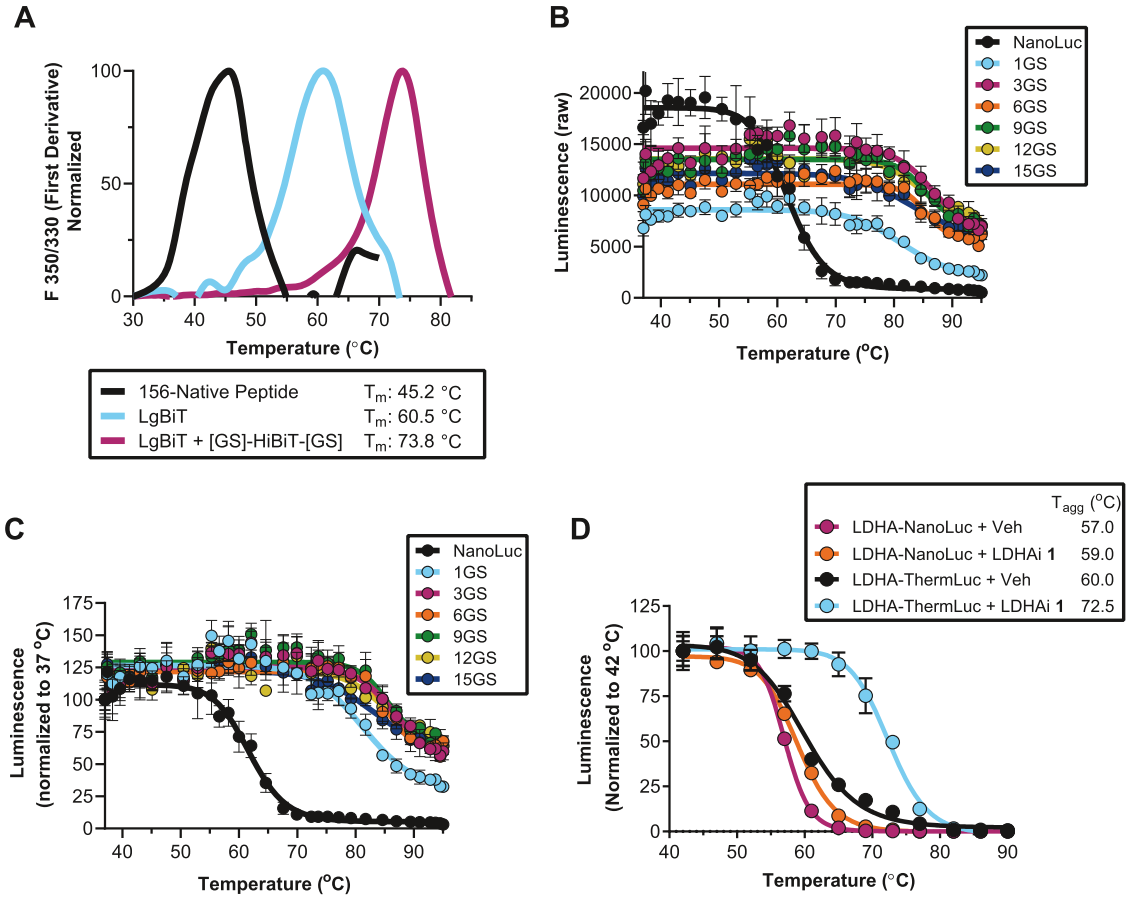

Figure 1. Engineering a thermally stable NLuc variant (ThermLuc). (A) Nano-differential scanning fluorimetry (nanoDSF) analysis of the thermal stability of reconstituted traditional NLuc (split into 156 and native peptide fragments), LgBiT, and LgBiT plus GS-HiBiT-GS peptide. (B,C) LgBiT and GS-HiBiT-GS fragments were combined into a single fusion protein and transiently expressed in HEK293T cells. Different Gly–Ser linker lengths to connect the fragments were examined. Graphs represent (B) raw luminescence values (mean ± SD, $n = 4$) and (C) luminescence normalized to the 37 °C signal (mean ± SD, $n = 4$). (D) Thermal shift expected from the binding of an LDHA inhibitor ($LDHA_i$) **1** is masked when using a LDHA-NLuc fusion but detectable with a LDHA-ThermLuc fusion (mean ± SD, $n = 4$).

protein and cellular debris are removed by centrifugation. The remaining soluble protein is then measured using a protein detection method, most commonly Western blot, though more recent methods have utilized mass spectrometry.[11−13] Label-free high-throughput CETSA methods have also proved valuable for target engagement studies where large compound sets can be screened against endogenous proteins without manipulation of the compound or protein; however, these techniques require high affinity antibodies and often need significant optimization for each target.[8,14,15]

Modernizing the CETSA approach for higher-throughput drug discovery applications requires the development of alternative CETSA-compatible detection methods, such as fluorescent and bioluminescent reporters.[16−18] One recent example was the development of a homogeneous bioluminescent assay using a split Nano luciferase reporter (SplitLuc CETSA). By appending a small HiBiT-based peptide reporter tag to the target and adding the complementary LgBiT protein with a furimazine substrate, SplitLuc CETSA allows for measurements in 384- and 1536-well microplates, providing an improvement in throughput.[19] In a similar approach, native Nano luciferase (NLuc) was fused to different targets to measure ligand-induced thermal shifts by detecting changes in the luminescent signal (NaLTSA).[20] To date, all CETSA methods perform end-point measurements, and so, independent samples are needed at each discrete temperature.[21] Moreover, classical CETSA analysis relies on single parameter methods using a sigmoidal fit of thermal response curves to calculate either the midpoint aggregation temperature (T_{agg}) or area-under-curve (AUC). Indeed, the limitations of high-throughput CETSA methods like SplitLuc and NaLTSA (NLuc CETSA) and the applied methodology to analyze thermal profiles, stem from the requirement to choose whether to examine either the dose–response of small molecules at a single temperature or a single concentration of drug over a range of temperatures.[15,19−23]

We reasoned that a real-time CETSA (RT-CETSA) assay, one that captures full thermal melt profiles of a target within living cells, would build upon previous CETSA iterations and enable the high-throughput acquisition of information-rich data across a temperature range from a single sample. We further reasoned that NLuc would be a favorable reporter tag for target proteins due to the low background luminescence, bright signal, and avoiding interference from intrinsic fluorescence of small molecules.[24] However, previous studies reported that purified NLuc has an aggregation temperature (T_{agg}) that ranges between 55 and 60 °C, precluding its use as a reporter for a portion of the proteome.[24−26] We hypothesized that a thermally stable NLuc variant would reduce the reporter's propensity to drive aggregation due to

https://doi.org/10.1021/acschembio.2c00334
ACS Chem. Biol. 2022, 17, 2471−2482

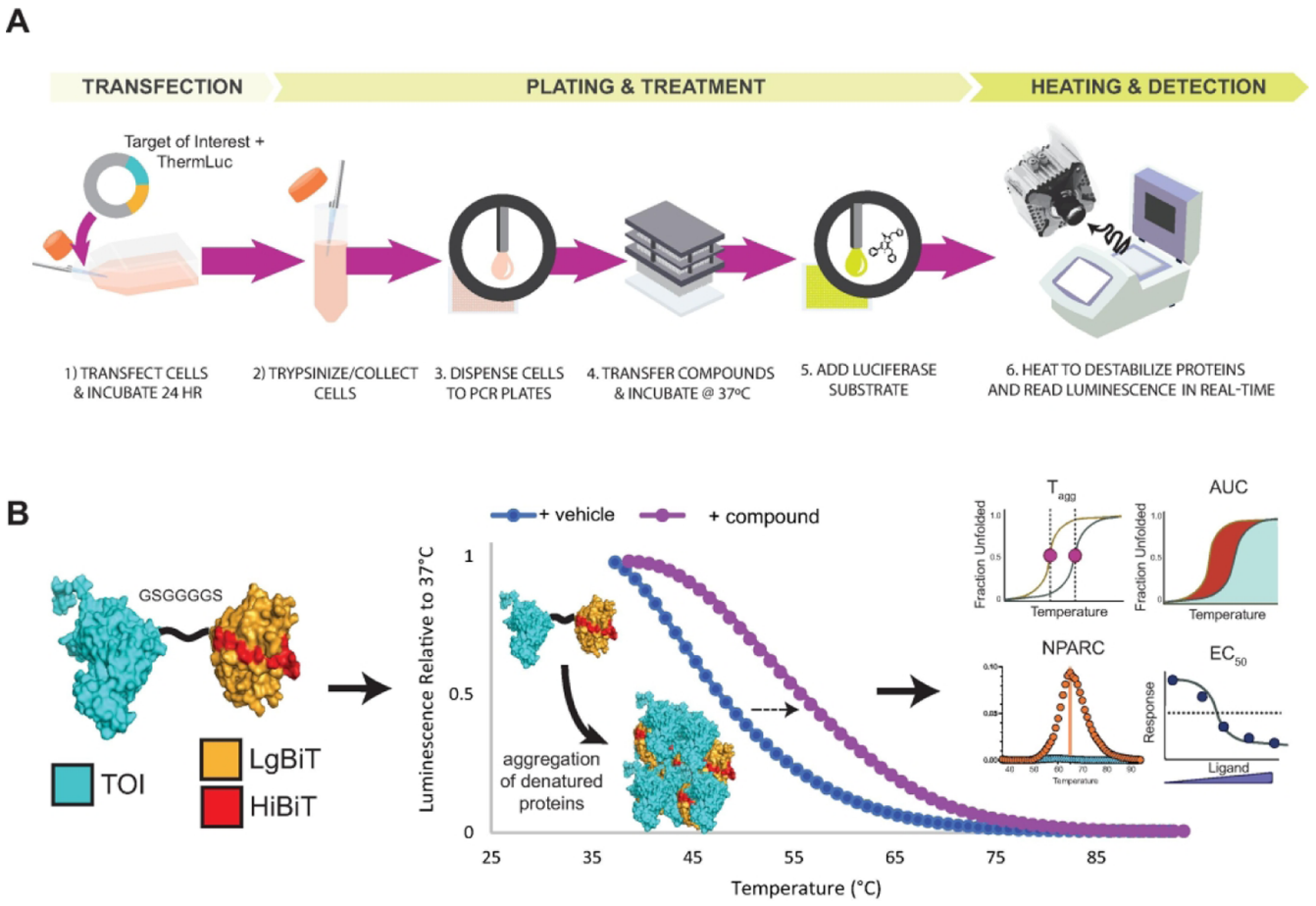

Figure 2. Real-time CETSA (RT-CETSA). (A) Schematic overview of the RT-CETSA approach. (B) Depiction of aggregation of ThermLuc-fusion protein at an elevated temperature, resulting in loss of luminescence. Target engagement is detected as a change in apparent T_{agg}, AUC, and novel nonparametric curve analyses (NPARC).

thermal unfolding, and that the NLuc variant LgBiT (11S), which was engineered to exhibit improved intracellular stability,[24] might exhibit the required higher thermal stability. Herein, we describe the bioengineering of thermally stable luciferase variants (ThermLuc) and the creation of a proof-of-concept RT-CETSA detection device. To quantify thermal unfolding in RT-CETSA, we also developed a novel approach using baseline-corrected thermal unfolding curves from MoltenProt, a recently developed analysis pipeline that produces nonlinear fits of protein unfolding, and goodness-of-fit tests between two models to determine thermal stabilizing molecules.[27] Herein, we describe the development of the RT-CETSA technology platform and its validation using lactate dehydrogenase alpha (LDHA)-ThermLuc fusions and a diverse set of pyrazole-based LDHA inhibitors.[28]

RESULTS AND DISCUSSION

Bioengineering Thermally Stable Luciferase Fusions.

A critical component of a CETSA approach capable of monitoring aggregation in real time would be the creation of a thermally stable luminescent reporter that continuously produces signal throughout a CETSA temperature ramp but does not drive reporter-led aggregation due to its own thermal unfolding. We hypothesized that an engineered NLuc using a LgBiT-based protein would be more thermally stable than traditional NLuc as well as have sufficient light emission to perform RT-CETSA. First, we measured the stability of purified LgBiT and HiBiT fragments against a thermal challenge using nanoDSF (Figure 1A). The thermal shift experiments revealed that combining LgBiT and HiBiT resulted in a significant T_{agg} shift to 73.8 °C compared to 45.2 °C for NLuc (using the corresponding 156 and native peptide fragments). This provided the rationale to generate plasmids encoding LgBiT and HiBiT assembled into a single fusion protein for heterologous expression in cells. Six constructs containing varying lengths of Gly−Ser linkers between LgBiT and HiBiT were transfected into HEK293T cells and assessed for both luminescence (Figure 1B) and thermal stability (Figure 1C). Although total luminescence was lower for samples expressing the LgBiT/HiBiT fusion proteins, they exhibited greater thermal stability, with an increase in T_{agg} from 63 °C (NLuc) to >90 °C. The construct with a single Gly−Ser peptide linker between luciferase fragments improved thermal stability compared to NLuc but to a lesser degree than the longer Gly−Ser linkers. We selected the fusion protein containing six Gly−Ser repeats, hereafter referred to as ThermLuc, for subsequent experiments measuring luminescence and thermal stability (Supporting Information Table S1).

To assess the utility of ThermLuc as a CETSA reporter, we created a fusion with LDHA, a 35 kDa soluble protein that aggregates in the low 60's °C. Small molecule-induced stabilization with 10 μM of LDHA inhibitor (LDHA$_i$) **1** was nearly undetectable under NaLTSA conditions, which is

https://doi.org/10.1021/acschembio.2c00334
ACS Chem. Biol. 2022, 17, 2471−2482

consistent with the unfolding of NLuc driving aggregation and masking the thermal stabilization effect of target engagement (Figure 1D). Swapping NLuc with the ThermLuc reporter slightly increased the apparent T_{agg} by 3.0 °C but showed a significant increase in thermal stability of the LDHA fusion with compound **1** (ΔT_{agg} = 12.5 °C). These data support the hypothesis that improved thermal stability of the luminescent reporter can unmask ligand-induced thermal stabilization of the target of interest, as the reporter no longer drives aggregation of the fusion protein due to its own thermal unfolding.

Real-Time CETSA Overview. To explore whether the entire aggregation profile of a target protein within its natural cellular environment could be monitored during heating, we pursued an RT-CETSA procedure utilizing the bioengineered ThermLuc protein (Figure 2). The method proceeds with the following steps: (1) cells are transfected with a plasmid encoding the target of interest (TOI) fused to ThermLuc, (2) cells expressing the ThermLuc fusion protein are dispensed into PCR plates and ligands are added, and (3) the luciferase substrate furimazine is added and luminescence is recorded kinetically as temperature is increased stepwise (e.g., 1 °C increments from 37 to 90 °C) to define the melt profile. The RT-CETSA method inherently requires a detection device that couples precise temperature control with a sensitive luminescence detection system (Supporting Information Figure S1). There is currently no instrument on the market that pairs these two components together. Modern qPCR machines are well suited for temperature control as they use thermal blocks with sub-centigrade precision and uniform heating across samples, but these machines are exclusively paired with detection systems optimized for fluorescence quantitation and not suitable for sensitive luminescence detection. Preliminary testing showed that an OEM qPCR instrument (LightCycler 480 II, Roche) was insensitive to luminescence signals that are in the working range of commonly used microplate readers (ViewLux, Pherastar). Therefore, we adapted the LightCycler 480 II to serve as the heating platform by removing the xenon bulb and emission filters from the light path and swapping the stock fluorescence camera with an Orca R2 CCD, which enabled detection of ThermLuc luminescence while heating (Supporting Information Figure S1). After performing an RT-CETSA experiment, analysis of the thermal unfolding profiles of ThermLuc-targets begins with automated pixel intensity analysis in MATLAB to extract raw luminescence values, followed by analysis of the melting curves using T_{agg}, AUC, and a novel nonparametric thermal curve analysis method to detect ligand-induced stabilization in RT-CETSA.

Real-Time Monitoring of NLuc Variant Fusions. The melting behavior of NLuc and ThermLuc luciferase fusion constructs was compared using a real-time detection approach. ThermLuc fusion proteins with three to fifteen Gly−Ser linker repeats between the HiBiT and LgBiT fragments showed significantly higher aggregation temperature (T_{agg}) compared to native NLuc when captured in real time (Supporting Information Figure S2A). Moreover, the reporter with a single Gly−Ser linker had a T_{agg} in between native NLuc and the ThermLuc constructs with longer linkers (Supporting Information Figure S2A), consistent with the behavior in the end-point luminescence lytic CETSA experiment (Figure 1C). Notably, the apparent T_{agg} in the RT-CETSA system may not align with T_{agg} values calculated using traditional luminescence or immunoblotting detection. Traditional CETSA utilizes a 3 min hold at a single temperature to calculate T_{agg}, as opposed to a rapid ramping and recording over a temperature range as in the real-time protocol. Additionally, the apparent T_{agg} in RT-CETSA is impacted by extrinsic factors that also contribute to luminescent signal, such as heat-induced substrate decomposition, which occurs at temperatures greater than 60 °C (Supporting Information Figure S2B). The decay rate of luminescence is largely attributable to temperature effects, where maintaining 37 °C throughout the RT-CETSA experiment shows minimal signal loss (Supporting Information Figure S2C). In our RT-CETSA experiments, the entire thermal melt profile of a target inside a live cell was recorded in less than 4 min, where 55 readings at discrete temperatures were captured from each well in 4 s intervals corresponding to Δ1 °C temperature increments.

Previous work on standardizing DSF protocols noted a phenomenon where T_m (melting profile) readouts are highly dependent on experimental parameters like ramp speed and temperature holds, but the ΔT_m induced by ligand binding remained constant.[29] In RT-CETSA, increasing the hold time of each temperature to 20 s reduced the T_{agg} of LDHA by Δ−16 °C, but the increased hold time did not significantly impact the compound-induced thermal shift (Supporting Information Figure S2D). RT-CETSA melt profiles therefore are not expected to align with absolute T_{agg} values calculated using traditional CETSA; rather, the primary goal of RT-CETSA is to identify thermal shifts due to ligand-induced stabilization. A 4 s hold at each temperature was sufficient to capture enough signal using the prototype detection system, while also limiting the decay rate of the furimazine substrate that would occur with longer holds. We expect that these hold times could be reduced further with a more sensitive camera, which would allow for faster ramping through a range of temperatures.

The nature of real-time measurements using a luciferase reporter requires the presence of a reporter substrate (furimazine) from the beginning time point, which presents additional experimental design considerations. The commercially available furimazine substrate typically used in NaLTSA experiments (Promega NanoGlo Substrate) is formulated in undisclosed chemical matter, and so, we examined whether using an alternative common solvent such as DMSO would be compatible with RT-CETSA. The melting profile of the ThermLuc fusion proteins and NLuc was very similar to that observed with the commercially available furimazine (Supporting Information Figure S2A,C). An additional consideration of including furimazine during heating is the potential for negative effects from the substrate on cell physiology. We performed a viability assay and found that cell growth was impaired with a 48 h treatment of the commercially available furimazine when used at concentrations 0.5× and higher, but not the DMSO-formulated furimazine up to 50 μM (Supporting Information Figure S2E). To further explore effects of furimazine on live cells, we performed a cell health screen using 0.005−100 μM of the DMSO-formulated furimazine in a SYSTEMETRIC cell health screening platform (AsedaSciences). The overall score in this assay placed furimazine in the "low cell stress" category, but effects on reactive oxygen species, membrane permeability, and nuclear membrane permeability were detected (Supporting Information Figure S2F). Importantly, the presence of furimazine during the heating step did not significantly alter target

https://doi.org/10.1021/acschembio.2c00334
ACS Chem. Biol. 2022, 17, 2471−2482

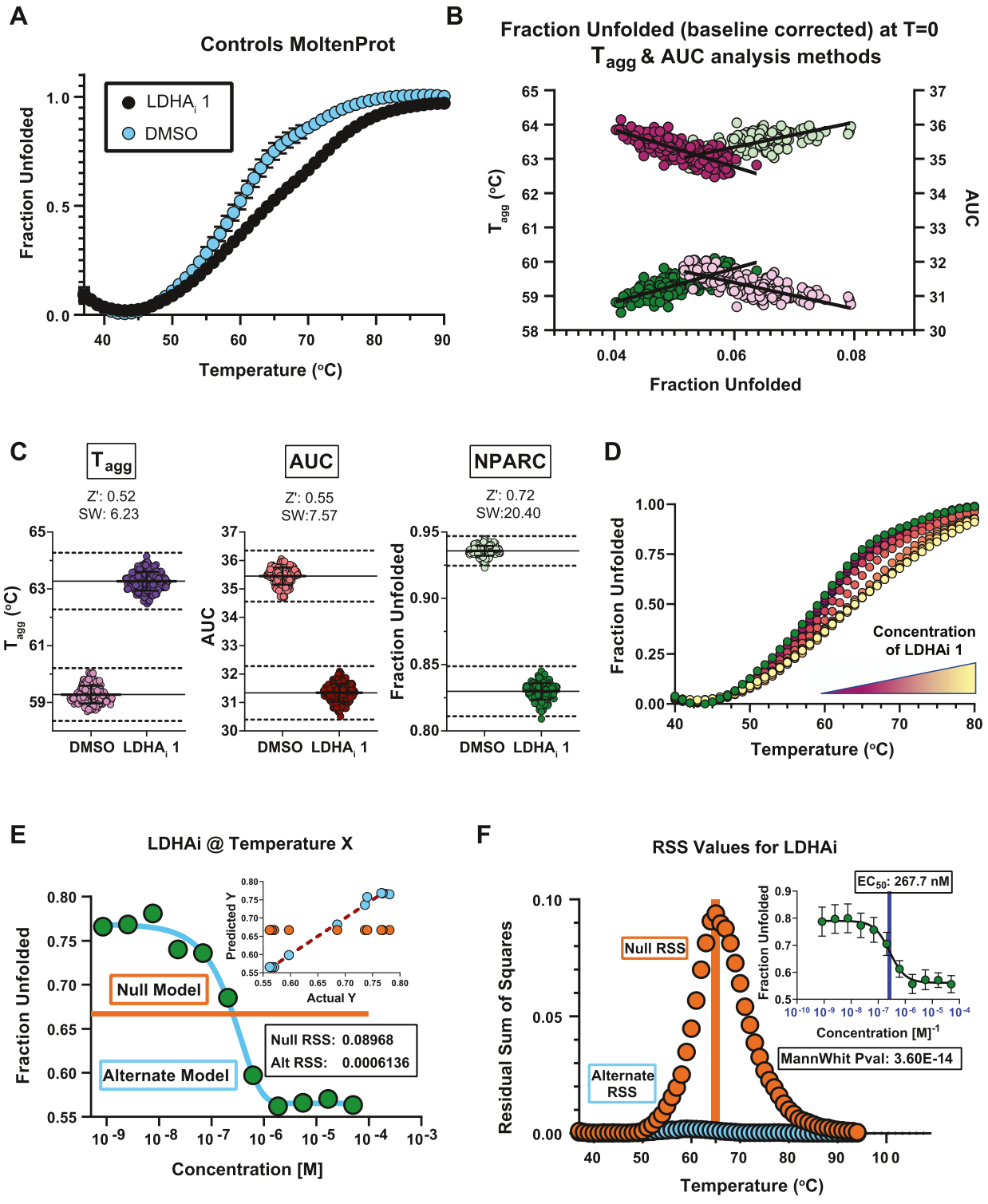

Figure 3. RT-CETSA thermal unfolding curves for LDHA-ThermLuc processed with MoltenProt. (A) Three biological replicate plates with N = 192 for each group per plate with standard deviation error bars. (B) Distribution of vehicle (lighter shade) and LDHA$_i$ **1** (darker shade) baseline-corrected fraction unfolded values at the first temperature point against T_{agg} (pink) and AUC (green) parameters from three biological replicate plates with N = 576 for each group. (C) Distributions of positive and negative controls using LDHA-ThermLuc are used to determine the Z′ statistic and signal window using T_{agg}, AUC, and NPARC methods of analysis. Solid lines represent the means of each group, and dashed lines represent the ±3 × SD for each control group. (D) Thermal dose−response curves of LDHA$_i$ **1** used for processing with MoltenProt and RT-CETSA scripts from the LDHA$_i$ experiment (vehicle control is green circles). (E) Goodness-of-fit tests for dose−response values at each temperature (green circles) are performed with a null (linear fit with a slope constrained to 0, orange) and alternative model (four-parameter log logistic fit, blue), from which the residual sum of squares (RSS) is calculated. Predicted vs actual Y values for each model are shown in the graph inset, showing the high degree of fit with the alternate model (blue circles) and the higher residuals for the poorly fit linear model (orange circles). (F) RSS values for the null (orange) and alternate (blue) models are plotted, and the difference in RSS between models is calculated. The point of

https://doi.org/10.1021/acschembio.2c00334
ACS Chem. Biol. 2022, 17, 2471−2482

Figure 3. continued

maximal RSS difference (orange bar) is used to determine EC_{50} of the compound, shown as the blue bar in the graph inset of concentration−response values.

engagement and thermal stabilization of LDHA (Supporting Information Figure S2G).

We next considered the rate of temperature increase that would bring the RT-CETSA system toward thermal equilibrium and properly capture aggregation profiles. Traditional CETSA protocols heat samples for 3−3.5 min, but there are a limited number of experiments that address whether this long incubation period is required. We performed end-point lytic CETSA with LDHA-ThermLuc and found that the melting profiles were similar after 30 s and 3.5 min of heating (Supporting Information Figure S2H). Next, we examined the rate of unfolding using RT-CETSA. RT-CETSA showed that thermal unfolding rapidly occurs upon the application of heat, as stable equilibrium of fraction unfolded is reached within 30 s of applying a 72 °C hold (Supporting Information Figure S2I). These results suggest that long incubation times, like those described in the original CETSA protocols,[8,9,16] are not required to detect compound-induced thermal shifts for all targets.

Target Engagement of LDHA-ThermLuc in RT-CETSA. Tangential work on thermal proteome profiling, a version of CETSA relying on mass-spectrometry as the method of readout, has used nonparametric analysis of response curves (NPARC) to integrate goodness of fits of the entire thermal response curve as an alternative to summary statistics like T_{agg}.[23,30] NPARC is more sensitive and specific to ligand-induced thermal stabilization than the melting point and other single-parameter values, and so, we sought to modify and integrate this method to analyze RT-CETSA data. Using MoltenProt analysis of the unfolded protein, we measured ligand-induced stabilization of LDHA across a temperature gradient (Figure 3A). To assess reproducibility of the RT-CETSA method, we examined 192 replicate wells of either DMSO or $LDHA_i$ **1** scattered across a 384-well plate. We observed a range of the fraction-unfolded values across the plate (DMSO: 0.063 ± 0.006 [9.45% CV], $LDHA_i$ **1**: 0.051 ± 0.005 [9.51% CV]), which may be attributable to experimental variability in cell number across wells (Figure 3B). Despite this variability, the starting luminescence did not affect the percent melt of LDHA-ThermLuc, and LDHAi **1** stabilization remained consistent, highlighting an advantage to capturing kinetic RT-CETSA data for every sample, where each sample can be normalized to its starting signal before heating (Figure 3B). Next, we compared each analysis method applicable to RT-CETSA data (T_{agg}, AUC, and NPARC) using the Z′ assay reproducibility statistic. Using DMSO vehicle as a negative control (N = 192) compared to LDHAi **1** treated wells as a positive control (N = 192), we found the best-performing Z′ to be NPARC [0.72] ≫ AUC [0.55] ≫ T_{agg} [0.52] (Figure 3C). The RT-CETSA thermal unfolding curve fitting approach also had acceptable signal windows with these controls (T_{agg}: 6.23, AUC: 7.57, and NPARC: 20.40) and a repeatable Δ4 °C compound-induced thermal shift across all wells (Figure 3C).

To assess real-time thermal shifts when compounds are tested across a concentration range, we modified the previous NPARC methods to create goodness-of-fit models for dose−response thermal melting curves, like the $LDHA_i$ **1** dose−response shown in Figure 3D, by fitting every concentration at every temperature with a null (linear fit with a slope of 0) and alternate (four-parameter log-logistic fit) model and then calculating the residual sum of squares (RSS) for each model fit (Figure 3E). The null fit is the theoretical model for when there is no dose-dependent stabilization of a target, in other words, no significant change to the melting profile of the target with ligand compared to a vehicle control. Thus, we expect to see a poorer fit of the null model, as compared to the alternate model, when dose-dependent stabilization of the target occurs, as illustrated by the actual versus predicted Y values for an $LDHA_i$ at a temperature near the aggregation temperature for LDHA (Figure 3E inset). A goodness-of-fit test of these residuals is performed with the nonparametric Mann Whitney U test against the model RSS values to detect significant binders (thermal shift/stabilization), and an EC_{50} is calculated for binders by analyzing dose−response curves at the point of maximal RSS difference using a four-parameter log-logistic fit (Figure 3F). We note that the point of maximal difference between null and alternate models is often at or near the T_{agg} for the target (Figure 3F).

RT-CETSA of LDHA Shows Compatibility Across Platforms. We benchmarked the RT-CETSA platform for its ability to guide structure−activity-relationship (SAR) studies on a set of 29 previously identified LDHA inhibitors, including 26 analogues of a class of pyrazole-based compounds, by comparing activity in complementary biochemical, biophysical, and phenotypic assays (Supporting Information Table S2). RT-CETSA experiments were performed by pre-incubating LDHA-ThermLuc transfected cells with compounds for 1 h in a dose-response ranging from micromolar to sub-nanomolar concentrations to determine EC_{50} values (Supporting Information Movie S1). A 1 h pre-incubation was chosen because a time course examination of $LDHA_i$ **1** showed diminished target engagement when compound pre-incubation was reduced to 15 min (Supporting Information Figure S2J). T_{agg}, AUC, and the modified NPARC analysis developed for RT-CETSA were compared to SplitLuc CETSA (isothermal heating performed at 61, 65, and 69 °C) and other biophysical and biochemical assays (Figure 4A, Supporting Information Figure S3A−C). We found that longer heating times in RT-CETSA (Figure S2D) or higher temperatures decreased the apparent potency for stabilization, as demonstrated by the SplitLuc CETSA where heating at 69 °C uniformly diminished potency compared to heating at 65 or 61 °C (Figure 4A, Supporting Information Table S2). These results further highlight the significant risk of missing target engagement events when using single end-point recordings if a non-optimal temperature is selected.

The RT-CETSA modified NPARC method derived a range of baseline-corrected fraction unfolded values from ∼0.5 to ∼0.8 for all LDHA inhibitors analyzed (Figure 4B). For each compound, EC_{50} values were calculated using the point of maximal difference between null and alternate models as previously shown in Figure 3F. In addition to a superior Z′ median for assay reproducibility, NPARC analysis was more sensitive and specific to ligand-induced thermal stabilization than T_{agg} or AUC (Figure 4A), highlighting the importance of the analysis methods. For example, compound **19** had an EC_{50}

https://doi.org/10.1021/acschembio.2c00334
ACS Chem. Biol. 2022, 17, 2471−2482

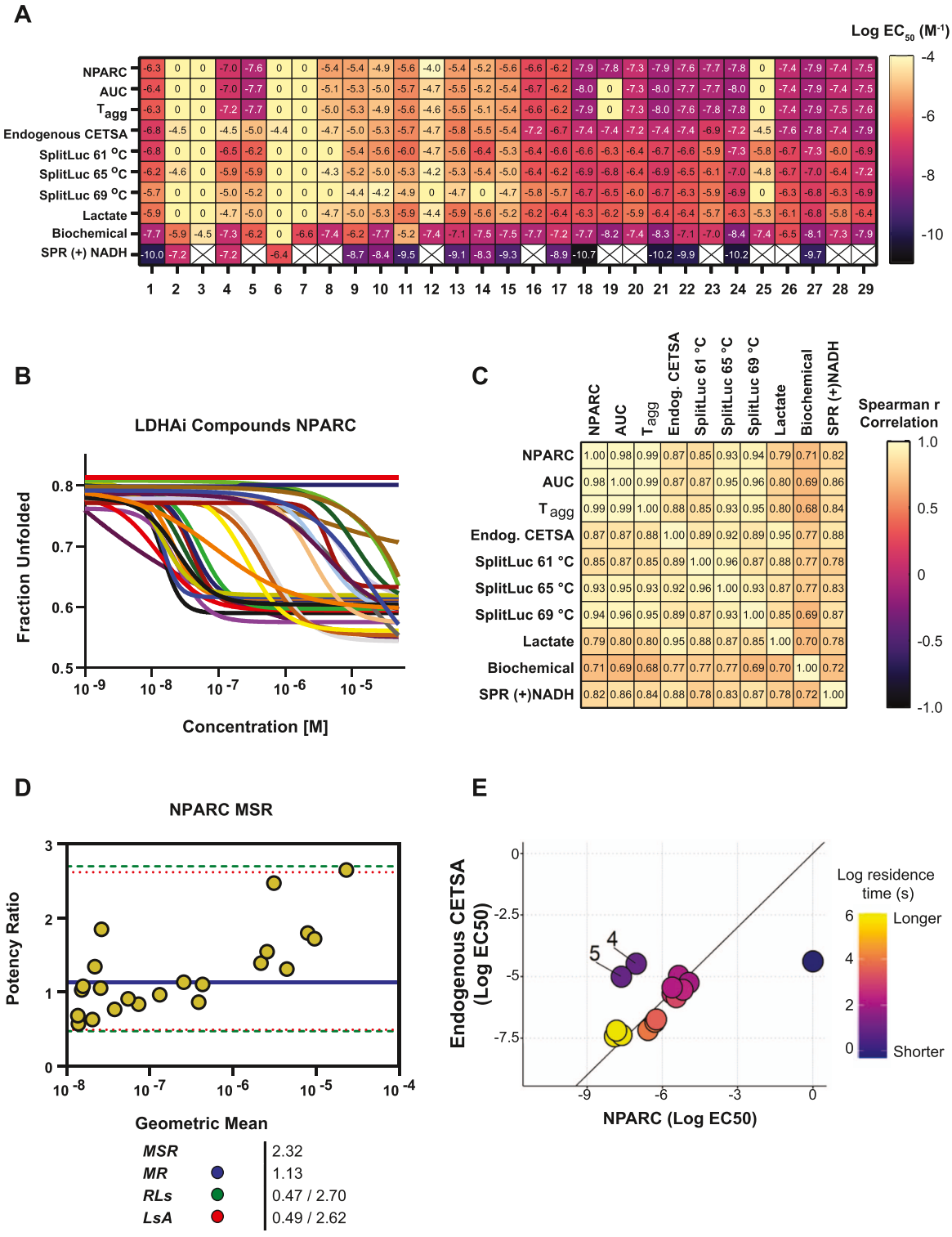

Figure 4. Correlative analysis of LDHA inhibitors. (A) EC_{50} values (log *M*) for plate containing 29 LDHA inhibitors ($N = 3$ replicates) analyzed using the following methods: RT-CETSA (4 s at each temperature), endogenous CETSA (71 °C × 3.5 min), SplitLuc CETSA (various temperatures, 3.5 min), lactate assay, biochemical assay, and surface plasmon resonance (SPR). Compounds with no detectable binding are annotated as "0", and compounds with no data are annotated with a blank square. (B) Dose−response curves for all LDHA inhibitors when using nonparametric curve (NPARC) analysis. NPARC derives fraction unfolded values for EC_{50} at the point of maximal difference between null and alternate models, presenting a range of fraction unfolded values from ∼0.8 for low concentrations of stabilizing small molecule to ∼0.5 for higher concentrations. (C) Spearman correlations of the compound rank order shows significant correlation among the methods tested. All correlations were statistically significant ($p < 0.005$, two-tail). (D) Testing of the minimum significant ratio (MSR) and related parameters further characterizes the high reproducibility of potency estimates from the RT-CETSA method. The mean ratio (MR) is shown as a solid blue line, limits of agreement (LsA) in dashed red lines, and ratio limits (RL) in dashed green lines. (E) Examination of NPARC EC_{50} values for compounds when tested in RT-CETSA versus acoustic endogenous CETSA. The color of the points indicates residence time, as calculated by SPR.

https://doi.org/10.1021/acschembio.2c00334
ACS Chem. Biol. 2022, 17, 2471−2482

value of 15 nM in RT-CETSA using NPARC but was inactive at 50 μM using conventional T_{agg} and AUC analysis. When comparing across different assays, most of the inhibitors with low nanomolar EC_{50} values in the biochemical assay using recombinant LDHA also had nanomolar EC_{50} values in the cellular-based SplitLuc CETSA and RT-CETSA target engagement assays using NPARC analysis. The rank order of the compounds was significantly correlated in the RT-CETSA assays using all three analysis methods when compared to SplitLuc and other biophysical/biochemical data (Figure 4C). RT-CETSA however, showed more potent response profiles compared to the SplitLuc CETSA approach that uses a 3.5 min heating step as an end point (Supporting Information Figure S3D). Absolute potencies were not identical across the assays. This is not surprising, as several studies have demonstrated that potency in isothermal CETSA is highly dependent on experimental conditions including duration of the heating step.[31,32]

Demonstrating on-target activity in cell-based models is a critical step in the development of small molecule probes and therapeutic candidates. Downstream validation of target engagement can be especially challenging when switching from biochemical assays to physiologically relevant cellular models. Many preclinical candidates fail because of off-target effects or poor physicochemical and pharmacokinetic properties.[33−35] This is exemplified within the set of LDHA inhibitors, where potency and the number of active analogues decreased as the complexity of the target's microenvironment increased from purified protein to cellular models (biochemical enzymatic assay vs cell-based lactate assay; SPR and DSF vs CETSA). For example, compound **15** had a biochemical enzymatic assay IC_{50} value of 30 nM, but its potency diminished in a cell-based lactate assay with an IC_{50} value of 6.5 μM and an RT-CETSA value of 2.5 μM by NPARC analysis. A common explanation is that biochemical, SPR, and DSF binding assays use recombinant protein and may overestimate the capacity of a molecule to engage a target within cells.

Correlative studies revealed that NPARC showed >95% overlap in identified "hits" compared to classical methods of CETSA analysis using AUC and T_{agg}. All three methods for analysis were tested for minimum significance ratio (MSR) and Z′ assay reproducibility calculations, two widely used measures of assay quality that describe separation between positive and negative controls.[36] Only NPARC (MSR: 2.32) and AUC (MSR: 2.67) methods were shown to reach acceptable reproducibility (Figure 4D, Supporting Information Figure S3E). By comparing goodness-of-fit tests for dose−response data across the entire melting curve, we captured treatment stabilization effects that were not detected by single summary statistics commonly used to describe thermal unfolding data. Moreover, SAR analysis of a set of LDHA inhibitors using the NPARC method supported previous studies that defined the importance of an ethyne linker between phenyl pyrazole and thiophene, or bioisosteric rings, as important for elevated intracellular and in vivo inhibitory activity.[28,37] This highlights the reliability of RT-CETSA to quantitatively determine SAR between sets of active and inactive analogues. We observed good correlation between potency of target engagement for RT-CETSA using NPARC and traditional CETSA using endogenous protein;[14] however, compounds **4,5** (different batches of the same compound) showed more potent stabilization in the RT-CETSA (Figure 4E). Compound **6** is another notable outlier; this compound showed poor activity in endogenous CETSA, SplitLuc, RT-CETSA, and the cellular lactate assay, suggesting that the potent activity that this compound showed against recombinant LDHA is lost in a cellular environment. As the RT-CETSA transitions through temperatures more rapidly (seconds) than traditional CETSA (minutes), the RT-CETSA method may provide an increased ability to detect engagement of compounds with faster off rates (as measured by SPR), such as compounds **4,5**. Moreover, the short duration at each temperature in RT-CETSA allows for the measurement of target engagement at higher temperatures before membrane integrity collapses. Using the same experimental conditions as for RT-CETSA, we measured HEK293T membrane integrity under rapid heating with propidium iodide, a dye that can only enter the cell and fluoresce when the cellular membrane is damaged (Figure S5). At 4 s holds for each temperature, permeability to propidium iodide was detected as an increase in fluorescence occurring at 68.5 °C.

Expanding the Utility of RT-CETSA for Multiple Targets. We hypothesized that we could leverage RT-CETSA to monitor the real-time melt profile of different targets simultaneously within a single plate. This would enable multiplexing of multiple targets, compounds, and concentrations within a single experimental plate, circumventing optimization for a discrete melting temperature and removing the risk of selecting a temperature where the thermal shift window would be missed. As a proof of concept, we used RT-CETSA to measure the thermal melt profile of eight different target-ThermLuc fusion proteins (Supporting Information Figure S4A). This set included immunotherapeutic targets currently marketed or in clinical trials (NGF, PCSK9, CD19, CD20, and PD1) and a set of in-house targets of interest (LDHA, cAbl, and DHFR) with known small molecule inhibitors.[19,37,38]

The entire melting profiles of these targets were visualized and recorded from the same plate, despite the narrow signal window afforded from our crudely assembled prototype detection device. Target engagement was observed for the cAbl-ThermLuc fusion using both dasatinib, a well-characterized cAbl orthosteric inhibitor, and GNF-2, a cAbl allosteric inhibitor (Supporting Information Figure S4B). We also explored DHFR thermal melt and target engagement using the RT-CETSA system because it had a known low melting temperature.[9,19] For DHFR, we observed a thermal stabilization conferred by the ThermLuc fusion, where only a partial aggregation profile was observed (Supporting Information Figure S4C). The thermal shift induced by the ligand methotrexate was detectable for DHFR-ThermLuc but smaller in magnitude when compared to DHFR-SplitLuc. Therefore, we hypothesized that the ThermLuc effects on DHFR thermal stability could be altered by varying the peptide linker between the two proteins. A set of 17 linkers with a range of predicted rigidity were constructed. Rigid polyproline-containing linkers further increased thermal stability of the DHFR-ThermLuc fusion protein. Some linkers reduced the overall thermal stability of the fusion protein; however, none fully recapitulated the melting behavior or thermal shift observed for DHFR with the small SplitLuc peptide tag (Supporting Information Figure S4D,E). Additional research is needed to define the intermolecular effects of ThermLuc on targets and its propensity to alter the inherent stability of its fusion partner.

https://doi.org/10.1021/acschembio.2c00334
ACS Chem. Biol. 2022, 17, 2471−2482

Our proof-of-concept studies indicate that RT-CETSA has the potential to serve as a multi-target platform that can rapidly assess EC_{50} values across a variety of different targets in parallel and can be used for SAR studies in medicinal chemistry campaigns. While these studies reveal promise in the approach, there are still hurdles related to the limited availability of commercial instrumentation that can couple precise temperature control and sensitive luminescence detection. If this obstacle can be resolved, the workflow and minimal hands-on requirements of the RT-CETSA method lend to a quick adaptation into a variety of applications, including characterizing chemical probes, lead optimization, identification of allosteric binders or starting points for PROTAC development,[39,40] and/or probing against multiple targets (e.g., family of proteins, anti-targets). The RT-CETSA prototype instrument enabled us to assess the melt profile of nine different protein targets simultaneously despite differences in starting luminescence, functional activity, and subcellular localization. We also demonstrated the compatibility of RT-CETSA to detect the melting profiles of secreted PCSK9 and NGF1 protein targets with no prior purification or enrichment of target needed. We anticipate that entire families of protein could be rapidly assessed for ligand binding under identical cellular conditions and provide valuable insights into off-target binding for sets of compounds. RT-CETSA may be particularly valuable for cellular proteins that are hard to "extract", such as nuclear proteins, using CETSA-compatible methods under non-denaturing conditions.[41] The RT-CETSA method has potential to capture the melting behavior of proteins in various subcellular compartments, provided that furimazine can access the target-ThermLuc fusion.

In the last decade, CETSA has become a valuable and widely implemented method for assessing target engagement in a cellular environment. All known CETSA methods involve endpoint lytic detection (Supporting Information Table S3) and either require high affinity antibodies or have a reliance on luciferase reporters like NLuc that can alter target biology and drive aggregation at temperatures lower than a target's inherent thermal properties.[13,14,24,25,42,43] While NLuc may be a suitable reporter in real-time target engagement studies for a majority of the proteome, the thermal and mechanical instability of the small and highly luminescent NLuc protein could impede the high-throughput transformation of CETSA for some targets with a high T_{agg}.[25,44] These issues led to the conceptual design and bioengineering of more thermally stable ThermLuc fusions as a reporter for RT-CETSA. We observed that the RT-CETSA method provided a robust approach to quantify ligand-induced stabilization of a well-characterized set of $LDHA_i$ analogues, supporting further development and implementation of this method as a high-throughput platform for SAR studies or screening applications. Importantly, RT-CETSA is prone to its own limitations and caveats, some of which are shared with traditional CETSA. For instance, some compounds that engage with a target do not affect its thermal stability, leading to false-negative results. Additionally, cellular membrane permeability was disrupted at temperatures greater than 68.5 °C, which can confound interpretations at high melting temperatures, which is also a caveat of traditional CETSA performed above 60 °C.[19,45,46] Similarly, higher temperatures are expected to alter the permeability of the furimazine substrate and enzymatic activity of the ThermLuc luciferase. We believe the impact of these factors can be minimized with proper controls and orthogonal screening methods. In summary, RT-CETSA provides an adaptable method that is broadly applicable for target engagement and screening campaigns, while offering sensitivity and ease of use that are unparalleled by current CETSA methods.

METHODS

Real-Time CETSA Assay. In the RT-CETSA procedure, we transiently and reverse transfected 7.5 million HEK293T cells using 7.5 μg of DNA and 15 μL of Lipofectamine 2000 (ThermoFisher) in a 25 cm^2 culture vessel. After 24 h, 5000 cells expressing the TOI-ThermLuc fusions were dispensed into 384-well PCR plates (10 μL per well) in CETSA buffer (phenol-free high glucose DMEM with sodium pyruvate and 1× Glutamax without FBS). 20 nL of compounds or DMSO vehicle controls was acoustically dispensed (Labcyte Echo) into the cells, and the plates were incubated for 1 h at 37 °C. 10 μL of 2× furimazine (diluted from Promega 50X stock into CETSA buffer) solution was added to each well. The plate was sealed and then run on a modified Roche LightCycler 480 II with a CCD camera to record luminescence kinetically as temperature increased stepwise (e.g., 1 °C increments from 37 to 90 °C). An optimal density was determined to ensure that the signal during heating would remain in the camera's linear detection range. The images taken were processed with a customized MATLAB script to extract the raw luminescence values from each well at each temperature.

Prototype RT-CETSA Hardware. All emission filters were removed from the light path in the Roche LightCycler 480 II, and the stock camera was swapped with an Orca II camera equipped with a Navitar 35 mm lens. Exposures were captured at user-defined intervals using LabView Software during the heating cycle, allowing for time to ramp and the time held at each step/°C; the thermal ramp was equal to the shutter speed of the camera (e.g., 2, 4, or 8 s). See the Supporting Information for additional details.

Melting Curve Analysis. Digital raw luminescence images from the RT-CETSA platform were analyzed using a customized MATLAB (The Mathworks, Inc.) script (public source file available at https://github.com/ncats/RT-CETSA-Analysis). See Supporting Information Methods for additional details on calibration, script parameters, thresholding, and corrections. Numerical values for mean signal intensity per signal region, mean local background intensity, and mean pixel intensity region minus local background were reported for each analyzed grid region, which were then processed using MoltenProt (CSSB, Hamburg Germany) software using the standard two-state unfolding model with 15 °C of the beginning and ending of curves used as initial values for baseline fit estimates. T_{agg} values were derived as the midpoint of the four-parameter sigmoidal curve fit of a baseline-corrected thermal unfolding curve. AUC values were calculated by processing the baseline-corrected curve fits using the auc function in the R package "MESS". All dose−response fits were calculated using a four-parameter log-logistic fit using the R package "drc" with 10,000 iterations to convergence. Nonparametric analysis of the thermal curves was performed by fitting two models to each dose−response at each data collection temperature point: (1) null model, which is a linear fit with a slope of 0, and (2) alternate model, which is a four-parameter log-logistic fit. The residual sum of squares was then calculated for each model across every temperature point, and a nonparametric Mann Whitney *U* test against model RSS values was performed to determine significant stabilization. EC_{50} values were then derived from curves that have significant stabilizers by fitting a four-parameter log-logistic fit using the curve values at the point of maximal RSS difference between null and alternate models[9,22,27,44] (public source file available at https://github.com/ncats/RT-CETSA-Analysis).

ASSOCIATED CONTENT

Supporting Information

The Supporting Information is available free of charge at https://pubs.acs.org/doi/10.1021/acschembio.2c00334.

https://doi.org/10.1021/acschembio.2c00334
ACS Chem. Biol. 2022, 17, 2471−2482

Description of the RT-CETSA prototype device, thermal stability data, examination of cellular membrane integrity during heating, and supplementary methods (PDF)

Coding sequences of various ThermLuc plasmids (unfused reporters, cloning acceptors, and fusion proteins) used in this study (XLSX)

Activity of LDHA inhibitors in biochemical, cell-based, and biophysical assays (XLSX)

Comparison of CETSA methods (XLSX)

Luminescence acquisition during RT-CETSA (MP4)

AUTHOR INFORMATION

Corresponding Author

Mark J. Henderson − *National Center for Advancing Translational Sciences, National Institutes of Health, Rockville, Maryland 20850, United States;* orcid.org/0000-0001-8590-7338; Email: mark.henderson2@nih.gov

Authors

Tino W. Sanchez − *National Center for Advancing Translational Sciences, National Institutes of Health, Rockville, Maryland 20850, United States;* orcid.org/0000-0002-2901-2211

Michael H. Ronzetti − *National Center for Advancing Translational Sciences, National Institutes of Health, Rockville, Maryland 20850, United States;* orcid.org/0000-0001-5034-7692

Ashley E. Owens − *National Center for Advancing Translational Sciences, National Institutes of Health, Rockville, Maryland 20850, United States*

Maria Antony − *National Center for Advancing Translational Sciences, National Institutes of Health, Rockville, Maryland 20850, United States*

Ty Voss − *National Center for Advancing Translational Sciences, National Institutes of Health, Rockville, Maryland 20850, United States*

Eric Wallgren − *National Center for Advancing Translational Sciences, National Institutes of Health, Rockville, Maryland 20850, United States*

Daniel Talley − *National Center for Advancing Translational Sciences, National Institutes of Health, Rockville, Maryland 20850, United States*

Krishna Balakrishnan − *National Center for Advancing Translational Sciences, National Institutes of Health, Rockville, Maryland 20850, United States*

Sebastian E. Leyes Porello − *National Center for Advancing Translational Sciences, National Institutes of Health, Rockville, Maryland 20850, United States*

Ganesha Rai − *National Center for Advancing Translational Sciences, National Institutes of Health, Rockville, Maryland 20850, United States;* orcid.org/0000-0001-9763-9641

Juan J. Marugan − *National Center for Advancing Translational Sciences, National Institutes of Health, Rockville, Maryland 20850, United States;* orcid.org/0000-0002-3951-7061

Samuel G. Michael − *National Center for Advancing Translational Sciences, National Institutes of Health, Rockville, Maryland 20850, United States*

Bolormaa Baljinnyam − *National Center for Advancing Translational Sciences, National Institutes of Health, Rockville, Maryland 20850, United States*

Noel Southall − *National Center for Advancing Translational Sciences, National Institutes of Health, Rockville, Maryland 20850, United States;* orcid.org/0000-0003-4500-880X

Anton Simeonov − *National Center for Advancing Translational Sciences, National Institutes of Health, Rockville, Maryland 20850, United States*

Complete contact information is available at: https://pubs.acs.org/10.1021/acschembio.2c00334

Author Contributions

†T.W.S. and M.H.R. contributed equally. T.W.S., M.H.R., A.E.O., S.E.L.P., N.S., and M.J.H. contributed to the bioengineering, experimentation, development, and analysis of the RT-CETSA data sets and methodology. T.W.S., M.H.R., A.E.O., K.B., G.R., J.J.M., S.G.M., B.B., A.S., and M.J.H. all contributed to the conceptual design of the RT-CETSA technology and platform. T.W.S., M.H.R., A.E.O., M.A., D.T., B.B., N.S., and M.J.H. contributed to the writing, figure generation, and editing of the manuscript. T.V. contributed to the creation of the MATLAB script used to analyze the luminescence signal. T.W.S., M.H.R., E.W., S.G.M., and M.J.H. contributed to the creation and optimization of the prototype RT-CETSA machine and analysis software. D.T. and G.R. contributed to the synthesis of the furimazine substrate and LDHA inhibitors.

Funding

This work was funded by the intramural research program at NCATS, NIH.

Notes

The authors declare the following competing financial interest(s): T.W.S., M.H.R., A.E.O., B.B., S.M., A.S. and M.J.H. are inventors on a patent: Real-Time Cellular Thermal Shift Assay (RT-CETSA) for Research and Drug Discovery (PCT/US21/45184). T.W.S., M.H.R., B.B. N.S., S.M. A.S., T.V., and M.J.H. are inventors on a related provisional patent: Methods and Systems for Analyzing Target Engagement Data from Biological Assays (HHS E-022-2022-0-US-01).

ACKNOWLEDGMENTS

We thank the NCATS compound management group for sourcing, quality control, formatting, and plating of compounds. We also thank K. Brimacombe for contributions to graphics.

REFERENCES

(1) Vidal, M.; Cusick, M. E.; Barabási, A.-L. Interactome Networks and Human Disease. *Cell* **2011**, *144*, 986−998.

(2) Ciulli, A. Biophysical screening for the discovery of small-molecule ligands. *Methods Mol. Biol.* **2013**, *1008*, 357−388.

(3) Edink, E.; Rucktooa, P.; Retra, K.; Akdemir, A.; Nahar, T.; Zuiderveld, O.; van Elk, R.; Janssen, E.; van Nierop, P.; van Muijlwijk-Koezen, J.; Smit, A. B.; Sixma, T. K.; Leurs, R.; de Esch, I. J. Fragment growing induces conformational changes in acetylcholine-binding protein: a structural and thermodynamic analysis. *J. Am. Chem. Soc.* **2011**, *133*, 5363−5371.

(4) Roy, M. J.; Winkler, S.; Hughes, S. J.; Whitworth, C.; Galant, M.; Farnaby, W.; Rumpel, K.; Ciulli, A. SPR-Measured Dissociation Kinetics of PROTAC Ternary Complexes Influence Target Degradation Rate. *ACS Chem. Biol.* **2019**, *14*, 361−368.

(5) Fedorov, O.; Niesen, F. H.; Knapp, S. Kinase inhibitor selectivity profiling using differential scanning fluorimetry. *Methods Mol. Biol.* **2012**, *795*, 109−118.

(6) Layton, C. J.; Hellinga, H. W. Thermodynamic Analysis of Ligand-Induced Changes in Protein Thermal Unfolding Applied to

High-Throughput Determination of Ligand Affinities with Extrinsic Fluorescent Dyes. *Biochemistry* **2010**, *49*, 10831−10841.
(7) Niesen, F. H.; Berglund, H.; Vedadi, M. The use of differential scanning fluorimetry to detect ligand interactions that promote protein stability. *Nat. Protoc.* **2007**, *2*, 2212−2221.
(8) Jafari, R.; Almqvist, H.; Axelsson, H.; Ignatushchenko, M.; Lundbäck, T.; Nordlund, P.; Molina, D. The cellular thermal shift assay for evaluating drug target interactions in cells. *Nat. Protoc.* **2014**, *9*, 2100−2122.
(9) Molina, D. M.; Jafari, R.; Ignatushchenko, M.; Seki, T.; Larsson, E. A.; Dan, C.; Sreekumar, L.; Cao, Y.; Nordlund, P. Monitoring Drug Target Engagement in Cells and Tissues Using the Cellular Thermal Shift Assay. *Science* **2013**, *341*, 84−87.
(10) Mateus, A.; Kurzawa, N.; Becher, I.; Sridharan, S.; Helm, D.; Stein, F.; Typas, A.; Savitski, M. M. Thermal proteome profiling for interrogating protein interactions. *Mol. Syst. Biol.* **2020**, *16*, No. e9232.
(11) Franken, H.; Mathieson, T.; Childs, D.; Sweetman, G. M.; Werner, T.; Tögel, I.; Doce, C.; Gade, S.; Bantscheff, M.; Drewes, G.; Reinhard, F. B.; Huber, W.; Savitski, M. M. Thermal proteome profiling for unbiased identification of direct and indirect drug targets using multiplexed quantitative mass spectrometry. *Nat. Protoc.* **2015**, *10*, 1567−1593.
(12) Friman, T. Mass spectrometry-based Cellular Thermal Shift Assay (CETSA(R)) for target deconvolution in phenotypic drug discovery. *Bioorg. Med. Chem.* **2020**, *28*, 115174.
(13) Mateus, A.; Hevler, J.; Bobonis, J.; Kurzawa, N.; Shah, M.; Mitosch, K.; Goemans, C. V.; Helm, D.; Stein, F.; Typas, A.; Savitski, M. M. The functional proteome landscape of Escherichia coli. *Nature* **2020**, *588*, 473−478.
(14) Owens, A. E.; Iannotti, M. J.; Sanchez, T. W.; Voss, T.; Kapoor, A.; Hall, M. D.; Marugan, J. J.; Michael, S.; Southall, N.; Henderson, M. J. High-Throughput Cellular Thermal Shift Assay Using Acoustic Transfer of Protein Lysates. *ACS Chem. Biol.* **2022**, *17*, 322−330.
(15) Shaw, J.; Leveridge, M.; Norling, C.; Karén, J.; Molina, D. M.; O'Neill, D.; Dowling, J. E.; Davey, P.; Cowan, S.; Dabrowski, M.; Main, M.; Gianni, D. Determining direct binders of the Androgen Receptor using a high-throughput Cellular Thermal Shift Assay. *Sci. Rep.* **2018**, *8*, 163.
(16) Henderson, M. J.; Holbert, M. A.; Simeonov, A.; Kallal, L. A. High-Throughput Cellular Thermal Shift Assays in Research and Drug Discovery. *SLAS Discov.* **2020**, *25*, 137−147.
(17) Kubota, K.; Funabashi, M.; Ogura, Y. Target deconvolution from phenotype-based drug discovery by using chemical proteomics approaches. *Biochim. Biophys. Acta, Proteins Proteomics* **2019**, *1867*, 22−27.
(18) Robers, M. B.; Dart, M. L.; Woodroofe, C. C.; Zimprich, C. A.; Kirkland, T. A.; Machleidt, T.; Kupcho, K. R.; Levin, S.; Hartnett, J. R.; Zimmerman, K.; Niles, A. L.; Ohana, R. F.; Daniels, D. L.; Slater, M.; Wood, M. G.; Cong, M.; Cheng, Y. Q.; Wood, K. V. Target engagement and drug residence time can be observed in living cells with BRET. *Nat. Commun.* **2015**, *6*, 10091.
(19) Martinez, N. J.; Asawa, R. R.; Cyr, M. G.; Zakharov, A.; Urban, D. J.; Roth, J. S.; Wallgren, E.; Klumpp-Thomas, C.; Coussens, N. P.; Rai, G.; Yang, S.-M.; Hall, M. D.; Marugan, J. J.; Simeonov, A.; Henderson, M. J. A widely-applicable high-throughput cellular thermal shift assay (CETSA) using split Nano Luciferase. *Sci. Rep.* **2018**, *8*, 9472.
(20) Dart, M. L.; Machleidt, T.; Jost, E.; Schwinn, M. K.; Robers, M. B.; Shi, C.; Kirkland, T. A.; Killoran, M. P.; Wilkinson, J. M.; Hartnett, J. R.; Zimmerman, K.; Wood, K. V. Homogeneous Assay for Target Engagement Utilizing Bioluminescent Thermal Shift. *ACS Med. Chem. Lett.* **2018**, *9*, 546−551.
(21) Seashore-Ludlow, B.; Axelsson, H.; Lundbäck, T. Perspective on CETSA Literature: Toward More Quantitative Data Interpretation. *SLAS Discov.* **2020**, *25*, 118−126.
(22) Massey, A. J. A high content, high throughput cellular thermal stability assay for measuring drug-target engagement in living cells. *PLoS One* **2018**, *13*, No. e0195050.
(23) Childs, D.; Bach, K.; Franken, H.; Anders, S.; Kurzawa, N.; Bantscheff, M.; Savitski, M. M.; Huber, W. Nonparametric Analysis of Thermal Proteome Profiles Reveals Novel Drug-binding Proteins. *Mol. Cell. Proteomics* **2019**, *18*, 2506−2515.
(24) Dixon, A. S.; Schwinn, M. K.; Hall, M. P.; Zimmerman, K.; Otto, P.; Lubben, T. H.; Butler, B. L.; Binkowski, B. F.; Machleidt, T.; Kirkland, T. A.; Wood, M. G.; Eggers, C. T.; Encell, L. P.; Wood, K. V. NanoLuc Complementation Reporter Optimized for Accurate Measurement of Protein Interactions in Cells. *ACS Chem. Biol.* **2016**, *11*, 400−408.
(25) Hall, M. P.; Unch, J.; Binkowski, B. F.; Valley, M. P.; Butler, B. L.; Wood, M. G.; Otto, P.; Zimmerman, K.; Vidugiris, G.; Machleidt, T.; Robers, M. B.; Benink, H. A.; Eggers, C. T.; Slater, M. R.; Meisenheimer, P. L.; Klaubert, D. H.; Fan, F.; Encell, L. P.; Wood, K. V. Engineered luciferase reporter from a deep sea shrimp utilizing a novel imidazopyrazinone substrate. *ACS Chem. Biol.* **2012**, *7*, 1848−1857.
(26) Sanchez, T. W.; Owens, A.; Martinez, N. J.; Wallgren, E.; Simeonov, A.; Henderson, M. J. High-Throughput Detection of Ligand-Protein Binding Using a SplitLuc Cellular Thermal Shift Assay. *Methods Mol. Biol.* **2021**, *2365*, 21−41.
(27) Kotov, V.; Mlynek, G.; Vesper, O.; Pletzer, M.; Wald, J.; Teixeira-Duarte, C. M.; Celia, H.; Garcia-Alai, M.; Nussberger, S.; Buchanan, S. K.; Morais-Cabral, J. H.; Loew, C.; Djinovic-Carugo, K.; Marlovits, T. C. In-depth interrogation of protein thermal unfolding data with MoltenProt. *Protein Sci.* **2021**, *30*, 201−217.
(28) Rai, G.; Brimacombe, K. R.; Mott, B. T.; Urban, D. J.; Hu, X.; Yang, S. M.; Lee, T. D.; Cheff, D. M.; Kouznetsova, J.; Benavides, G. A.; Pohida, K.; Kuenstner, E. J.; Luci, D. K.; Lukacs, C. M.; Davies, D. R.; Dranow, D. M.; Zhu, H.; Sulikowski, G.; Moore, W. J.; Stott, G. M.; Flint, A. J.; Hall, M. D.; Darley-Usmar, V. M.; Neckers, L. M.; Dang, C. V.; Waterson, A. G.; Simeonov, A.; Jadhav, A.; Maloney, D. J. Discovery and Optimization of Potent, Cell-Active Pyrazole-Based Inhibitors of Lactate Dehydrogenase (LDH). *J. Med. Chem.* **2017**, *60*, 9184−9204.
(29) Baljinnyam, B.; Ronzetti, M.; Yasgar, A.; Simeonov, A. Applications of Differential Scanning Fluorometry and Related Technologies in Characterization of Protein-Ligand Interactions. *Methods Mol. Biol.* **2020**, *2089*, 47−68.
(30) Perrin, J.; Werner, T.; Kurzawa, N.; Rutkowska, A.; Childs, D. D.; Kalxdorf, M.; Poeckel, D.; Stonehouse, E.; Strohmer, K.; Heller, B.; Thomson, D. W.; Krause, J.; Becher, I.; Eberl, H. C.; Vappiani, J.; Sevin, D. C.; Rau, C. E.; Franken, H.; Huber, W.; Faelth-Savitski, M.; Savitski, M. M.; Bantscheff, M.; Bergamini, G. Identifying drug targets in tissues and whole blood with thermal-shift profiling. *Nat. Biotechnol.* **2020**, *38*, 303−308.
(31) Jarzab, A.; Kurzawa, N.; Hopf, T.; Moerch, M.; Zecha, J.; Leijten, N.; Bian, Y.; Musiol, E.; Maschberger, M.; Stoehr, G.; Becher, I.; Daly, C.; Samaras, P.; Mergner, J.; Spanier, B.; Angelov, A.; Werner, T.; Bantscheff, M.; Wilhelm, M.; Klingenspor, M.; Lemeer, S.; Liebl, W.; Hahne, H.; Savitski, M. M.; Kuster, B. Meltome atlas-thermal proteome stability across the tree of life. *Nat. Methods* **2020**, *17*, 495−503.
(32) Määttä, T. A.; Rettel, M.; Sridharan, S.; Helm, D.; Kurzawa, N.; Stein, F.; Savitski, M. M. Aggregation and disaggregation features of the human proteome. *Mol. Syst. Biol.* **2020**, *16*, No. e9500.
(33) Morgan, P.; Van Der Graaf, P. H.; Arrowsmith, J.; Feltner, D. E.; Drummond, K. S.; Wegner, C. D.; Street, S. D. Can the flow of medicines be improved? Fundamental pharmacokinetic and pharmacological principles toward improving Phase II survival. *Drug Discov. Today* **2012**, *17*, 419−424.
(34) Vinegoni, C.; Dubach, J. M.; Thurber, G. M.; Miller, M. A.; Mazitschek, R.; Weissleder, R. Advances in measuring single-cell pharmacology in vivo. *Drug Discov. Today* **2015**, *20*, 1087−1092.
(35) Walker, D. K. The use of pharmacokinetic and pharmacodynamic data in the assessment of drug safety in early drug development. *Br. J. Clin. Pharmacol.* **2004**, *58*, 601−608.

https://doi.org/10.1021/acschembio.2c00334
ACS Chem. Biol. 2022, 17, 2471−2482

(36) Zhang, J. H.; Chung, T. D.; Oldenburg, K. R. A Simple Statistical Parameter for Use in Evaluation and Validation of High Throughput Screening Assays. *J. Biomol. Screen* **1999**, *4*, 67−73.
(37) Rai, G.; Urban, D. J.; Mott, B. T.; Hu, X.; Yang, S. M.; Benavides, G. A.; Johnson, M. S.; Squadrito, G. L.; Brimacombe, K. R.; Lee, T. D.; Cheff, D. M.; Zhu, H.; Henderson, M. J.; Pohida, K.; Sulikowski, G. A.; Dranow, D. M.; Kabir, M.; Shah, P.; Padilha, E.; Tao, D.; Fang, Y.; Christov, P. P.; Kim, K.; Jana, S.; Muttil, P.; Anderson, T.; Kunda, N. K.; Hathaway, H. J.; Kusewitt, D. F.; Oshima, N.; Cherukuri, M.; Davies, D. R.; Norenberg, J. P.; Sklar, L. A.; Moore, W. J.; Dang, C. V.; Stott, G. M.; Neckers, L.; Flint, A. J.; Darley-Usmar, V. M.; Simeonov, A.; Waterson, A. G.; Jadhav, A.; Hall, M. D.; Maloney, D. J. Pyrazole-Based Lactate Dehydrogenase Inhibitors with Optimized Cell Activity and Pharmacokinetic Properties. *J. Med. Chem.* **2020**, *63*, 10984−11011.
(38) Contreras, P. S.; Gonzalez-Zuñiga, M.; González-Hódar, L.; Yáñez, M. J.; Dulcey, A.; Marugan, J.; Seto, E.; Alvarez, A. R.; Zanlungo, S. Neuronal gene repression in Niemann-Pick type C models is mediated by the c-Abl/HDAC2 signaling pathway. *Biochim. Biophys. Acta* **2016**, *1859*, 269−279.
(39) Vogelmann, A.; Jung, M.; Hansen, F. K.; Schiedel, M. Comparison of Cellular Target Engagement Methods for the Tubulin Deacetylases Sirt2 and HDAC6: NanoBRET, CETSA, Tubulin Acetylation, and PROTACs. *ACS Pharmacol. Transl. Sci.* **2022**, *5*, 138−140.
(40) Chernobrovkin, A. L.; Cázares-Körner, C.; Friman, T.; Caballero, I. M.; Amadio, D.; Martinez Molina, D. A Tale of Two Tails: Efficient Profiling of Protein Degraders by Specific Functional and Target Engagement Readouts. *SLAS Discov.* **2021**, *26*, 534−546.
(41) Scheer, U.; Kartenbeck, J.; Trendelenburg, M. F.; Stadler, J.; Franke, W. W. Experimental disintegration of the nuclear envelope. Evidence for pore-connecting fibrils. *J. Cell Biol.* **1976**, *69*, 1−18.
(42) Nagasawa, I.; Muroi, M.; Kawatani, M.; Ohishi, T.; Ohba, S. I.; Kawada, M.; Osada, H. Identification of a Small Compound Targeting PKM2-Regulated Signaling Using 2D Gel Electrophoresis-Based Proteome-wide CETSA. *Cell Chem. Biol.* **2020**, *27*, 186−196.
(43) Savitski, M. M.; Reinhard, F. B.; Franken, H.; Werner, T.; Savitski, M. F.; Eberhard, D.; Molina, D.; Jafari, R.; Dovega, R. B.; Klaeger, S.; Kuster, B.; Nordlund, P.; Bantscheff, M.; Drewes, G. Tracking cancer drugs in living cells by thermal profiling of the proteome. *Science* **2014**, *346*, 1255784.
(44) Ding, Y.; Apostolidou, D.; Marszalek, P. Mechanical Stability of a Small, Highly-Luminescent Engineered Protein NanoLuc. *Int. J. Mol. Sci.* **2020**, *22*, 55.
(45) Bischof, J. C.; Padanilam, J.; Holmes, W. H.; Ezzell, R. M.; Lee, R. C.; Tompkins, R. G.; Yarmush, M. L.; Toner, M. Dynamics of cell membrane permeability changes at supraphysiological temperatures. *Biophys. J.* **1995**, *68*, 2608−2614.
(46) McNulty, D. E.; Bonnette, W. G.; Qi, H.; Wang, L.; Ho, T. F.; Waszkiewicz, A.; Kallal, L. A.; Nagarajan, R. P.; Stern, M.; Quinn, A. M.; Creasy, C. L.; Su, D. S.; Graves, A. P.; Annan, R. S.; Sweitzer, S. M.; Holbert, M. A. A High-Throughput Dose-Response Cellular Thermal Shift Assay for Rapid Screening of Drug Target Engagement in Living Cells, Exemplified Using SMYD3 and IDO1. *SLAS Discov.* **2018**, *23*, 34−46.

https://doi.org/10.1021/acschembio.2c00334
ACS Chem. Biol. 2022, 17, 2471−2482